Journal of Catalysis 394 (2021) 58–66

Contents lists available at ScienceDirect

Journal of Catalysis

journal homepage: www.elsevier.com/locate/jcat

Limitations of identical location SEM as a method of degradation studies on surfactant capped nanoparticle electrocatalysts

Yuhui Hou [a,1,*], Noémi Kovács [a,b,1], Heng Xu [c], Changzhe Sun [a], Rolf Erni [d], María de Jesús Gálvez-Vázquez [a], Alain Rieder [a], Huifang Hu [a], Ying Kong [a], Menglong Liu [a], Benjamin J. Wiley [c], Soma Vesztergom [a,b,*], Peter Broekmann [a]

[a] University of Bern, Department of Chemistry and Biochemistry, Freiestrasse 3, 3012 Bern, Switzerland
[b] Eötvös Loránd University, Department of Physical Chemistry, Pázmány Péter sétány 1/A, 1117 Budapest, Hungary
[c] Duke University, Department of Chemistry, French Family Science Cen 2214, NC–27708 Durham, NC, USA
[d] Swiss Federal Laboratories for Materials Science and Technology (EMPA), Electron Microscopy Center, Überlandstrasse 129, CH–8600 Dübendorf, Switzerland

ARTICLE INFO

Article history:
Received 14 October 2020
Revised 11 December 2020
Accepted 12 December 2020
Available online 23 December 2020

Keywords:
Electrocatalysis
CO_2 reduction
Electron microscopy
Under-beam contamination
Carbon
Polyvinylpyrrolidone (PVP)

ABSTRACT

Identical location scanning electron microscopy (IL–SEM) has become an important tool for electrocatalysis research in the past few years. The method allows for the observation of the same site of an electrode, often down to the same nanoparticle, before and after electrochemical treatment. It is presumed that by IL–SEM, alterations in the surface morphology (the growth, shrinkage, or the disappearance of nanosized features) can be detected, and the thus visualized degradation can be linked to changes of the catalytic performance, observed during prolonged electrolyses. In the rare cases where no degradation is seen, IL–SEM may provide comfort that the studied catalyst is ready for up-scaling and can be moved towards industrial applications. However, although it is usually considered a non-invasive technique, the interpretation of IL–SEM measurements may get more complicated. When, for example, IL–SEM is used to study the degradation of surfactant-capped Ag nanocubes employed as electrocatalysts of CO_2 electroreduction, nanoparticles subjected to the electron beam during pre-electrolysis imaging may lose some of their catalytic activity due to the under-beam formation of a passive organic contamination layer. Although the entirety of the catalyst obviously degrades, the spot mapped by IL–SEM reflects no or little changes during electrolysis. The aim of this paper is to shed light on an important limitation of IL–SEM: extreme care is necessary when applying this method for catalyst degradation studies, especially in case of nanoparticles with surface-adsorbed capping agents.

1. Introduction

Due to the ever-increasing consumption of fossil fuels, gigatons of CO_2 are released yearly to the atmosphere, expediting global warming [1]. A possible way of mitigating the effects of atmospheric CO_2 is to reduce it electrochemically. Electrochemical reduction does not only allow CO_2 to be regarded as a valuable raw material instead of an environmentally dangerous waste, but it may also provide a solution for the storage of excess renewable (hydro-, solar or wind) energy [2].

Mostly due to this, electrochemical CO_2 reduction —a process that was first described more than 150 years ago [3]— has recently become the forefront of electrochemical research [4]. Searching for the term "electrochemical CO_2 reduction" on the website of ACS Publications yields 3334 research papers about this topic, only from the past year; Google Scholar, when searched for the same term and for the same period of time, gives $>$ 17000 matches. A majority of these publications are original research papers that describe new catalyst materials, which —somewhat remarkably— all exhibit excellent qualities when applied for CO_2 reduction. This means that by covering electrodes with the newly invented catalysts, and carrying out electrolyses of solutions that contain CO_2 dissolved in some form, high current densities of CO_2 reduction can be achieved at relatively low overpotentials, and the process may in an ideal case yield only one or just a few desired products [4].

* Corresponding authors at: University of Bern, Department of Chemistry and Biochemistry, Freiestrasse 3, 3012 Bern, Switzerland (Y. Hou); Eötvös Loránd University, Department of Physical Chemistry, Pázmány Péter sétány 1/A, 1117 Budapest, Hungary (S. Vesztergom).
E-mail addresses: yuhui.hou@dcb.unibe.ch (Y. Hou), vesztergom@chem.elte.hu (S. Vesztergom), peter.broekmann@dcb.unibe.ch (P. Broekmann).
[1] These authors contributed equally.

https://doi.org/10.1016/j.jcat.2020.12.006
0021-9517/

Compared to the tremendous amount of research invested in the design of new electrocatalyst materials for CO_2 electroreduction, technologies that operate on an industrial scale are still rare. Undoubtedly, the most important obstacle that hinders the application of newly developed catalysts on an industrial level is an issue of stability: catalysts that may show remarkable features in lab experiments tend to degrade and lose their performance over prolonged use. This may especially be true for catalysts owing their activity to a fine structure, such as colloidally synthesized nanoparticles that are especially prone to degradation over long-time operation. In case of these catalysts, studying (electro-)mechanical degradation and its effects on the catalytic performance has to be the first step of technological up-scaling.

Although many *operando* techniques (*e.g.*, X-ray diffraction, scattering or absorption, as well as Raman spectroscopies [5,6]) can provide an insight to nanoparticle transformations occurring during CO_2 reduction, it is still more common to use *ex situ* electron microscopic (EM) techniques to observe, in particular, the structural changes that electrocatalysts suffer during CO_2 reduction.

In order to apply EM in an electrocatalysis study, the catalyst has to be sampled before and after it is made subject to electrochemical treatment. When comparing images taken before and after electrolysis, we usually work under two implicit assumptions: *(i.)* that the areas scanned before and after the electrolysis are either physically the same, or are both representative of the sample as a whole; and *(ii.)* that any changes we observe are indeed caused by the electrochemical treatment and not by other operations, *e.g.,* the pre-electrolysis scanning of the sample, careless sample transportation, exposition to air or to chemicals, etc.

The former of the above two assumptions can readily be made explicit, for example, if identical location scanning or transmission electron microscopies (IL–SEM or IL–TEM) are employed. IL–TEM was first described by a work of Mayrhofer et al. in 2008 [7], and the first report on the application of IL–SEM by Hodnik et al. [8] followed not much later, in 2012. In early studies, the catalyst material was loaded on a TEM finder grid (made of gold) to facilitate identical location imaging [7]. Later it was found that it is enough to apply a small incision (a cross-like scratch) on other (*e.g.*, graphite) holders to relocate the scanned site after electrolysis, which rendered the use of finder grids unnecessary. Due to the fact that IL–EM is able to visualize changes of a catalyst surface, often down to the details of individual nanoparticles, IL–EM found immediate application in catalyst degradation studies on a variety of target reactions [9,10].

In the field of CO_2 electrolysis, IL–EM became a prominent method of studying catalyst degradation [11–21], mainly because it is considered (and, starting from its discovery, often advertised as) a non-destructive method. It is usually assumed that if a given catalyst preserves good performance characteristics over longer periods of electrolysis, and neither IL–SEM nor IL–TEM reveal any structural degradation, the catalyst is stable and can be considered a potential candidate for up-scaled (*e.g.*, flow cell) studies [15].

Unfortunately, however, the situation is not this simple, especially because, in some cases, the pre-electrolysis EM imaging does affect the future catalytic performance of the sampled catalyst areas. For example, in the literature of IL–TEM studies of electrocatalysts, there are reports on the electron beam induced shrinkage (as well as some ripening) of Pt nanoparticles used in fuel cells [22]. Based on these results, Arenz and Zana strongly recommend that in order to check if the electron beam changes the sample, TEM analysis following the electrochemical measurements should also be performed at pristine locations; *i.e.*, locations which have not been previously exposed to the electron beam [23].

For IL–SEM, probably based on the assumption that the electron dose is much lower than in the case of TEM, no such warning was given, and it is indeed not likely that the beam used under SEM conditions could induce similar sintering effects observed in TEM. The sintering of nanoparticles may however not be the only way an electron beam can alter a catalyst surface: another, equally important phenomenon —namely, the under-beam formation of a passive layer— should also deserve attention.

That electron bombardment of a conducting sample *in vacuo*, where only slightest traces of organic vapours occur, can result in the coverage of the sample with a non-conducting layer of polymerized carbon compounds was first noticed by Lariviere Stewart [24] in 1934 — that is, four years before von Ardenne built the first SEM [25]. That electron bombardment, especially during focusing, can also cause changes to the surface of a sample inside an SEM was first noticed as early as 1946 by Marton et al. [26]. Recently, two reviews from Postek et al. [27,28] discussed some issues of interpreting SEM images: the second part [28] was entirely devoted to the issue of electron beam-induced specimen contamination.

Postek et al. [28] pointed out that the origin of beam-induced contaminations can both be the sample itself and the vacuum system of the SEM. While the cleanliness of the latter can be significantly improved (for example, by the replacement of diffusion pumps with turbomolecular ones backed by dry backing pumps in modern instruments), the history of the specimen prior to entering the vacuum system still remains important [28]. In case of samples with significant organic content, organic molecules remaining on the sample surface can break, undergo polymerization, and get "pinned" to the sample by the beam during scanning [28]. Depending on the electron dose, the formed carbonaceous layer can grow at a rate of a few nanometers/seconds over the sample surface, even if only low accelerating voltages are used.

It is interesting to note that although under-beam contamination is a well-studied subject in the literature of SEM (see [27,28], as well as the references cited therein), studies on the effect of under-beam contamination/passivation on the future electrochemical behaviour of the sample are scarce, and are mostly focused on corrosion and not on electrocatalytic properties [29]. Yet, as we are going to demonstrate in this paper, under-beam passivation can practically disable the sampled part of a catalyst, especially if it contains organic remnants (capping agents) from the synthesis process. While other parts of the catalyst (not affected by the electron beam before electrolysis) remain active and very often degrade significantly during the catalysed process, the part of the sample affected by pre-electrolysis scanning remains intact, and probably entirely passive, due to the carbonaceous film formed on it under the beam.

Here we demonstrate, by IL–SEM studies on polyvinylpyrrolidone (PVP) functionalized Ag nanocubes used as electrocatalysts for CO_2 reduction, a catalytic activity disabling effect of a passive carbonaceous layer that is known to be formed under the electron beam during pre-electrolysis SEM scans [30]. The aim of this paper is to emphasize the necessity of extreme care being taken not to misinterpret IL–SEM studies that seemingly demonstrate excellent catalyst stability.

2. Experimental

Catalyst preparation. Ag nanocubes (Ag NCs) were prepared by an upscaled synthesis route described elsewhere [31]. As support, a glassy carbon plate (2 mm thickness, Alfa Aesar, type 1) was mirror-polished (0.5 μm alumina suspension, Buehler), was thoroughly rinsed with ultrapure water and ethanol, dried, and masked with an inert PTFE tape to leave an 0.8 cm × 1 cm geometric surface area open for catalyst coating.

In order to form a carbon-supported Ag NC catalyst, 5.6 mg of the as-prepared Ag nanocubes [31] (in the form of powder) was dispersed in 6 cm^3 isopropanol (VLSI Selectipur, BASF) by a 1-hour sonication. 1.5 mg of technical carbon powder (Vulcan XC 72R, Cabot, USA) was also dispersed in 3 cm^3 isopropanol by 1-hour of sonication, and the two suspensions were subsequently mixed by sonicating for 30 min. The resulting suspension was dried overnight under vacuum conditions, yielding a C-supported Ag NC catalyst powder. This powder was re-dispersed in 1.5 cm^3 of isopropanol containing 75 $\mu\ell$ of a Nafion solution (Aldrich, 5 wt% dissolved in a mixture of lower aliphatic alcohols and water). The obtained dispersion was subjected to sonication for 30 min, and for each electrode, 25 $\mu\ell$ of the resulted ink was drop-cast onto the glassy carbon plate and dried in a vacuum oven.

An Ag NC catalyst without carbon support was prepared by dispersing 22 mg of the as-prepared Ag NCs in 6 cm^3 isopropanol by 1-hour sonication and spin-coating 75 $\mu\ell$ of this suspension onto a glassy carbon support in three steps over 1 minute, using 1000 min^{-1} rotation rate on an Ossila spin coater.

Both the C-supported and the unsupported Ag NC catalysts were exposed to a UV-ozone atmosphere (PSD Series, Novascan, operated with air at atmospheric pressure) for 12 min.

For studies on a gas diffusion electrode (GDE, experimental details were described elsewhere [15]) the suspension of carbon-supported Ag NCs was drop-cast on the hydrophobic surface of a Sigracet 39 BC (Fuel Cell Store) GDE, and the nanocubes were percolated through the porous body of the GDE by a vacuum filtration system placed on the rear side of the electrode, followed by air-drying at ambient conditions lasting 30 min. No UV-ozone treatment was applied to the thus prepared, Ag NC-modified GDE. The GDE was used as part of the gas flow cell described in [15], combined with a Sustainion alkaline membrane (X37-50 RT, Dioxide materials) and an anode compartment containing 2 mol dm^{-3} KOH solution.

XPS Characterization. X-ray photoelectron spectroscopy (XPS) studies were carried out using a Thermo ESCALAB 250 XI instrument at a pass energy of 30 eV using monochromated Al K-α line ($h\nu = 1486.7$ eV). Charge correction was based on the position of the C*1s* peak (284.8 eV). The XPS spectra were subjected to a Shirley background subtraction and were analysed using the CasaXPS software.

Electrocatalysis studies. For all electrochemical experiments, a potentiostat/galvanostat (Metrohm Autolab 302N, The Netherlands) was used to control the potential, current density, and transferred charge. The electrolysis experiments were carried out using a custom-built, air-tight, H-type glass cell. Apart from the working electrode that was prepared as described above, the three-electrode arrangement consisted of a "leakless" Ag|AgCl|3 mol dm^{-3}KCl reference (Pine) and a Pt-foil (1.5 cm × 0.5 cm, Goodfellow) counter electrode. For electrolyses, 0.5 mol dm^{-3} $KHCO_3$ (ACS grade, Sigma-Aldrich) electrolyte solutions were prepared with ultrapure water (Milli-Q by Merck Millipore) and were saturated with CO_2 (99.999%, Carbagas, Switzerland). During the experiments, continuous gas flow was maintained through the electrolyte solution. To avoid possible fluctuations in CO_2 solubility caused by a change in the ambient temperature, all electrochemical experiments were performed at 20 °C, by immersing the H-type cell into a thermostated water bath. Automatic *IR* compensation was applied following the determination of the cell resistance by positive feedback. For the sake of comparability, all potentials given herein were converted to the reversible hydrogen electrode (RHE) scale. The reported current densities were normalized to the geometric surface area.

Gaseous products generated in the cell were detected by connecting the purging gas outlet to a GC analyzer (SRI Instruments Multigas Analyzer Nº3). The continuous flow of the carrier CO_2 gas through the electrolysis cell carried volatile reaction products from the head-space into the sampling loops of the gas chromatograph. The partial current I_i, corresponding to the formation of a gaseous product *i*, can be calculated [32] as

$$I_i = x_i n_i F v_m, \quad (1)$$

where x_i denotes the mole fraction of the products, determined by GC using an independent calibration standard gas (Carbagas); n_i is the number of electrons involved in the reduction reaction to form a particular product ($n = 2$ for both CO and H_2 formation); $F = 96485.3$ C mol^{-1} is Faraday's constant; and v_m is the molar CO_2 gas flow rate measured by a universal flowmeter (7000 GC flowmeter, Ellutia) at the exit of the electrochemical cell.

The Faradaic efficiency (*FE*) of a given reaction product can be determined by dividing the respective partial current, determined from Eq. (1), by the total current measured electrochemically. A thermal conductivity detector (TCD, for the detection of H_2) and a flame ionization detector (FID, for the detection of CO) were applied in our studies. We found that in the studied system H_2 and CO are the only two detectable products, accounting for 100% ± 5% of the current density that was electrochemically measurable. The electrochemically measured current densities were thus subdivided into partial current densities by taking into account the chromatographically determined concentration ratios, as will be shown later in Fig. 2. During operation, aliquots were analysed in intervals of 20 min during steady state electrolyses.

EM Measurements. EM analysis was conducted with a Zeiss Gemini 450 SEM with an InLens secondary electron (SE) and a backscatter electron detector (BSD). An accelerating voltage of 1.5 kV (probe current of 20 pA) and 5.0 kV (probe current of 120 pA) were applied for SE and BSD imaging, respectively. For high-angle annular dark-field scanning transmission electron microscopy (HAADF–STEM) combined with energy-dispersive X-ray spectroscopy (EDX) and TEM imaging, an FEI Titan Themis (equipped with a SuperEDX detector) was used with an acceleration voltage of 300 kV.

3. Results and discussion

In colloidal nanoparticle synthesis, PVP is a widely applied shape-control agent that promotes the growth of specific crystal faces while hindering others [33,34]. In the synthesis of Ag NCs used in this study, PVP —by strongly binding to the (100) facets of Ag—, facilitated the formation of almost perfect nanocubes of side lengths of about 100 nm, as shown in Fig. 1a. The XPS spectrum (Fig. 1b) of a catalyst prepared without carbon support clearly exhibits a strong Ag*3d* signal, as well as a small peak that can be assigned to the N*1s* excitation of the PVP molecules adsorbed on the surface of the nanocubes. As shown in Fig. 1b, the applied UV-ozone treatment resulted in a significantly decreased N*1s* peak intensity. The peak has not disappeared, however, which hints that some PVP still remained on the surface despite the UV-ozone treatment.

Although the adsorbed PVP could, in principle, inhibit the catalytic activity of the nanocubes [35,36], the UV-ozone treated, C-supported Ag NCs showed good performance when applied for the electroreduction of CO_2. This is demonstrated by Fig. 2a, showing the current density and the product distribution as a function of the applied electrode potential. The current densities shown in Fig. 2a were averaged for 1-hour electrolyses carried out in CO_2 saturated 0.5 mol dm^{-3} $KHCO_3$ solutions: for the electrolyses at different potentials, fresh solutions and newly prepared catalysts were applied.

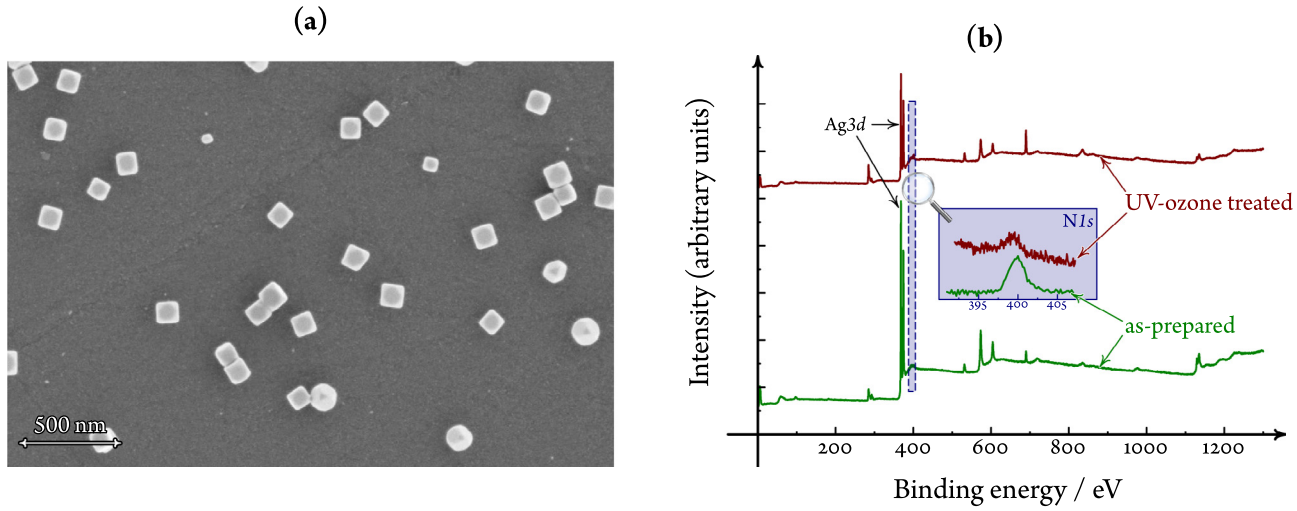

Fig. 1. Scanning electron micrograph **(a)** and X-ray photoelectron survey **(b)** of the unsupported Ag NC catalyst. XPS spectra are shown in **(b)** for the as-prepared catalyst (green curve) and for the catalyst made subject to UV-ozone treatment (red curve) as well. (For interpretation of the references to colour in this figure legend, the reader is referred to the web version of this article.)

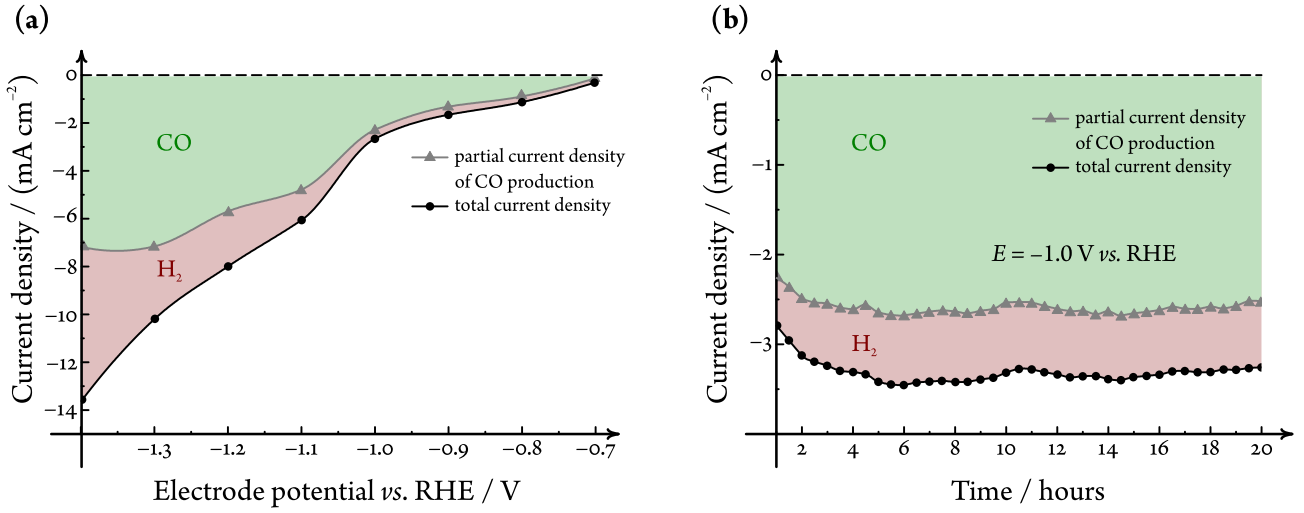

Fig. 2. The electrocatalytic performance of carbon-supported Ag nanocubes, used as catalysts of CO_2 electroreduction in a CO_2-saturated 0.5 mol dm^{-3} $KHCO_3$ solution. **(a)** Potential dependence of the current density and the product distribution, as determined by means of online gas chromatography in an H-type cell for 1-hour electrolyses. Each electrolysis (data points) were carried out using a freshly prepared catalyst and a fresh solution. Curves were created by interpolation. **(b)** Time dependence of the catalytic performance, as determined by a single electrolysis experiment lasting 20 hours, with subsequent chromatographic head-space analysis (data points). The curve was created by interpolation.

It is known that on Ag, the primary product of CO_2 reduction is CO [37]. The same is true for the carbon-supported Ag NCs, with the addition that compared to plain silver —*e.g.*, a silver foil [14]— the Ag nanocubes exhibit a broader overpotential range for CO production. That is, only a little amount of H_2 is formed at potentials less negative than −1.1 V *vs.* RHE, and CO_2 reduction generally prevails over hydrogen evolution in the entirety of the studied potential range ($-1.3\ \text{V} < E < -0.7\ \text{V}$). This observation is in agreement with other reports on nanoparticulate silver catalysts of CO_2 electroreduction [38].

In order to check the stability of the catalyst, we chose the moderate potential value of −1.0 V *vs.* RHE for a prolonged operation study. As shown in Fig. 2b, the catalyst preserved both its overall activity and its relative selectivity towards the production of CO (the Faradaic efficiency of CO formation was about 80%) for an electrolysis lasting 20 hours.

Nevertheless, since catalysts can maintain their macroscopic activity even as they undergo partial deactivation or decomposition [39], we carried out IL–SEM investigations of the working electrode surface, which —although the overall activity remained unchanged— indeed revealed some degradation.

In Fig. 3 we compare two scanning electron micrographs of the same spot of a working electrode surface; one recorded before (Fig. 3a) and one after (Fig. 3b) a 20-hours electrolysis treatment at −1.0 V *vs.* RHE, similar to the one used to obtain the data of Fig. 2b. Fig. 3a shows highly isotropic Ag NCs of a side length of about 100 nanometers, distributed evenly on the supporting carbon matrix. As revealed by Fig. 3b, the nanocubes undergo some slight deformation and shrinkage during electrolysis, and, more prominently, some subnanometer sized particles appear on the surface. EDX mapping (Fig. 3c) confirmed that these small particles consist of silver, and are most probably formed as a debris of nanoparticle degradation due to the mechanical impact of gas evolution [16].

In order to get a clearer view of the degradation process of Ag NCs, the above SEM experiment was repeated with a working elec-

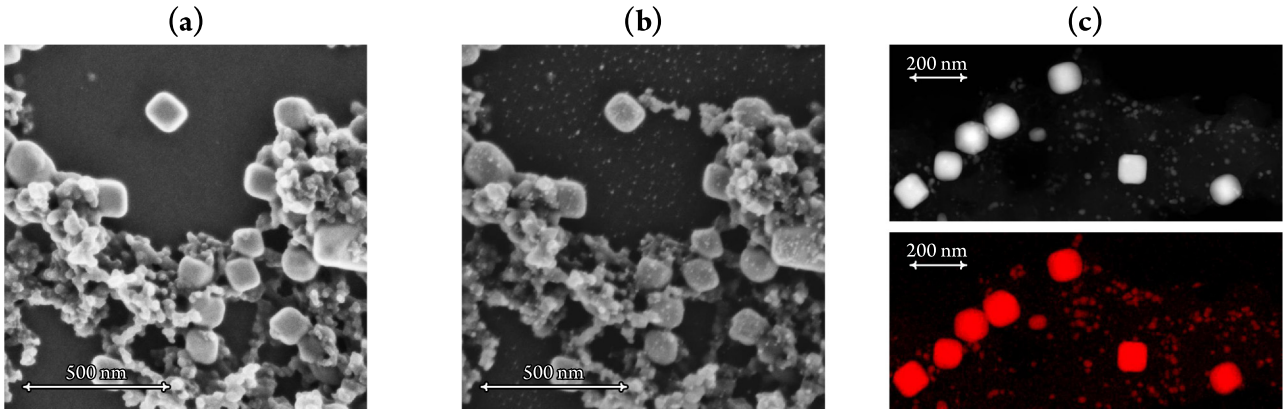

Fig. 3. IL–SEM investigation of the degradation of carbon-supported Ag nanocubes, used as catalysts of CO_2 electroreduction. The same spot of the working electrode surface is shown just before **(a)** and right after **(b)** the electrode was used for a 20-hours electrolysis of a CO_2-saturated 0.5 mol dm^{-3} $KHCO_3$ solution at an electrode potential of −1.0 V *vs.* RHE. The formation of subnanometer sized Ag particles during electrolysis is revealed by the HAADF–STEM (gray-scale) and EDX scans (red-scale) in **(c)**, recorded post-electrolysis at a pristine location that has not been subjected to an electron beam before.

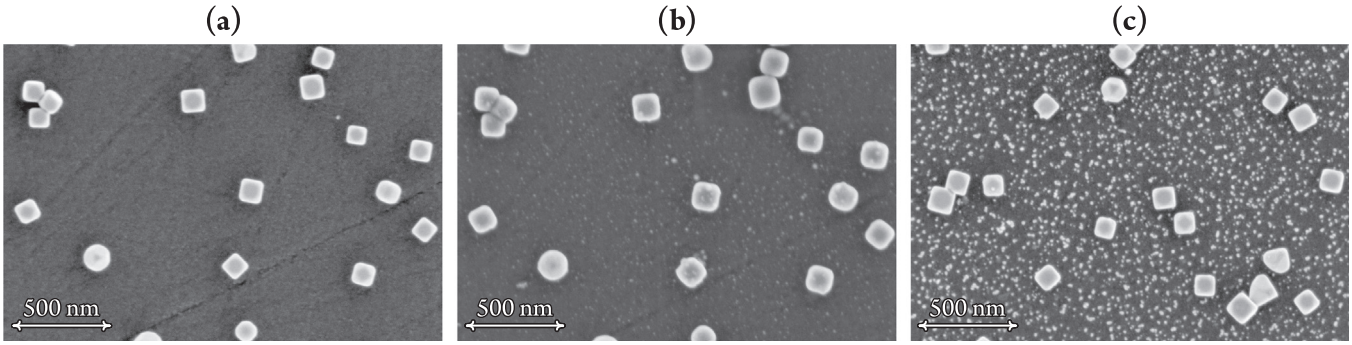

Fig. 4. SEM investigation of the degradation of non-supported Ag nanocubes, used as catalysts of CO_2 electroreduction. The same spot of the working electrode surface is shown just before **(a)** and right after **(b)** the electrode was used for a 20-hours electrolysis of a CO_2-saturated 0.5 mol dm^{-3} $KHCO_3$ solution. A different spot of the same sample is shown after electrolysis in **(c)**.

trode prepared without the supporting carbon matrix (see the Experimental section for details).

The as-prepared electrode surface is shown in Fig. 4a, exhibiting cubic shaped Ag nanoparticles distributed on the glassy carbon electrode substrate. Somewhat surprisingly, the SEM image of the same spot, recorded after a 20-hours electrolysis, shows practically no degradation and the appearance of just a little amount of the subnanometer sized particles, as shown in Fig. 4b. What is even more surprising is that if we record an SEM micrograph with the same configuration, just of a different spot of the sample —that was not scanned before electrolysis—, the picture gets quite different. Fig. 4c clearly shows slightly deformed Ag nanocubes, along with a significant amount of Ag debris formed during electrolysis.

The micrographs of Fig. 4 very clearly reveal an important pitfall of IL–SEM analysis; namely, that due to electron beam-induced changes of the catalyst surface during the pre-electrolysis scan, the sample may get at least partially deactivated for the catalysed process. Due to its decreased electrocatalytic activity, the pre-scanned area of the sample may show no or little changes during the electrolytic process, while other spots (that were not affected by pre-electrolysis SEM scanning) preserve their activity and, in turn, exhibit significant degradation. In other words, the often advertised nondestructiveness of IL–SEM [8,9] should not be taken as granted — at least, not for all catalyst types.

That the effect shown in Fig. 4 can indeed be explained by pre-electrolysis electron beam–sample interactions is further demonstrated by Fig. 5, showing an SEM micrograph of a working electrode surface obtained after electrolysis. Only a part (a rectangular segment) of this sample was scanned by SEM before electrolysis took place, and despite that the sample was exposed

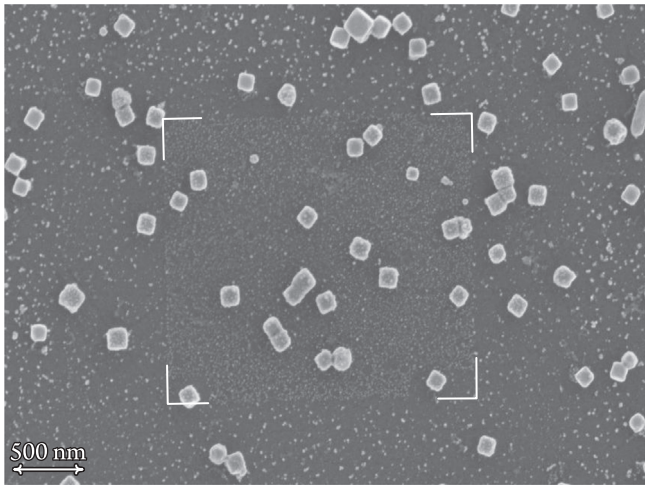

Fig. 5. SEM micrograph of a sample of non-supported Ag NC catalyst taken after a 40-hours electrolysis at −1 V *vs.* RHE in a CO_2-saturated 0.5 mol dm^{-3} $KHCO_3$ solution. A rectangular segment of the sample —shown in the image by its corners— was also scanned before electrolysis. This pre-scanned area exhibits different degradation features compared to the rest of the surface.

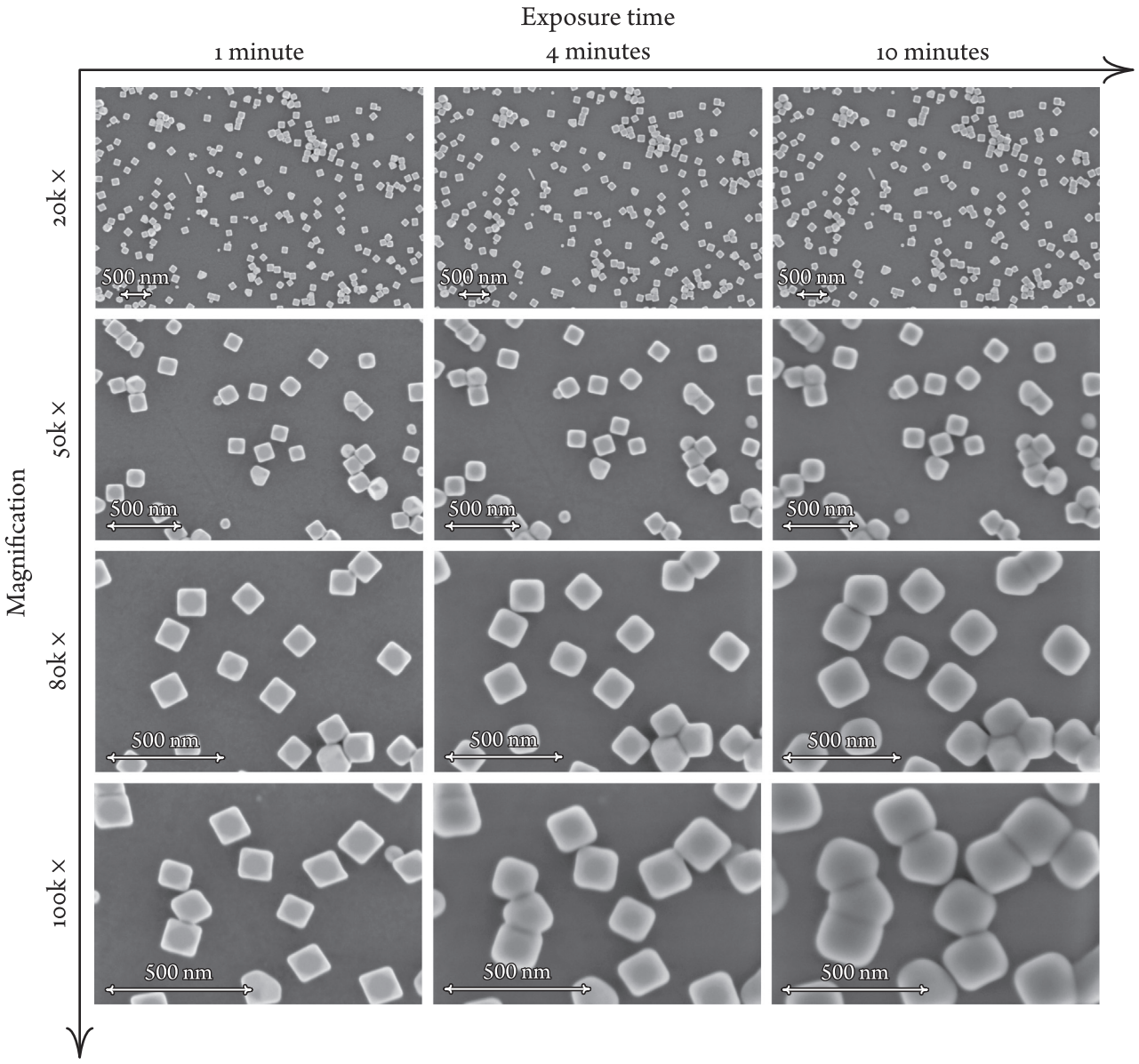

Fig. 6. SEM micrographs of a catalyst surface, obtained using different magnifications and after different scanning times. The applied accelerating voltage was 1.5 kV.

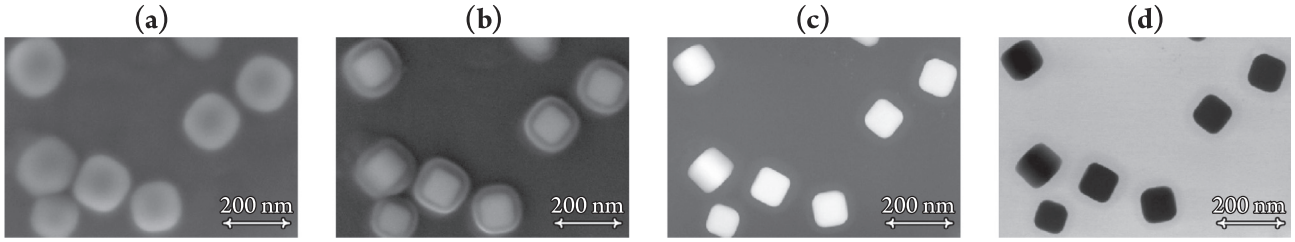

Fig. 7. Electron microscopic images of Ag NCs after electron beam irradiation was carried out for 10 min with a scanning electron beam of 1.5 kV accelerating voltage. **(a)** Secondary electron SEM image taken at 1.5 kV acceleration voltage. **(b)** Secondary electron SEM image obtained at 20 kV. **(c)** HAADF–STEM image taken at 300 kV. **(d)** TEM bright field image taken at 300 kV.

to the electron beam only for a short time, a marked difference can be observed between the degradation features of the pre-scanned segment and the rest of the surface area. Most notably, the coverage of the pre-scanned area with the subnanometer sized Ag particles is less pronounced, compared to other sites. This hints that the electron beam exerts an effect not only on the Ag nanoparticles but also on the underlying glassy carbon substrate.

Note that provided we refrain from long-time exposure of the sample to the electron beam, the above-described electron beam irradiation effect is hardly noticeable *per se*. Yet, as shown by Fig. 5, even the irradiation damages that remained undetected dur-

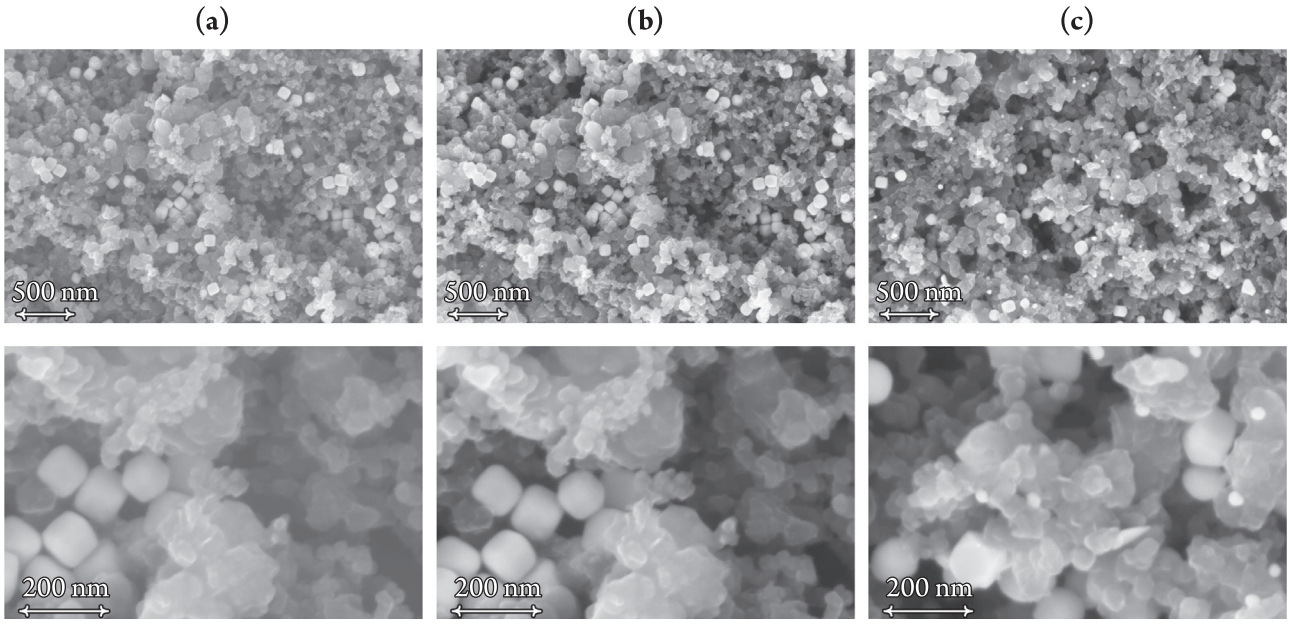

Fig. 8. SEM micrographs of different magnification of a GDE modified by Ag NCs. Identical locations are shown prior to **(a)** and after **(b)** a potentiostatic electrolysis at −2.0 V *vs.* an Ag | AgCl | 3 mol dm^{-3} KCl(aq) reference electrode consuming 1600 C cm^{-2}. A different location is shown after the electrolysis in **(c)**.

ing pre-electrolysis EM scanning can prove significant when the sample is used for electrolysis and scanned afterwards.

To demonstrate the irradiation effect in itself, we carried out prolonged SEM scans on one of our catalyst samples. As revealed by Fig. 6, the effect of contamination (as visualized by the growth and even the apparent merging of the nanocubes) is more pronounced when larger magnifications are applied (*i.e.*, when the beam is more focused) or when the sample is scanned for longer times.

At first glance, the growing and subsequently merging nanocubes shown in Fig. 6 may resemble the coalescence of Pt nanoparticles observed by Chorkendorff et al. under *in situ* TEM conditions [22]. Note, however, that under TEM conditions, the accelerating voltage and the electron dose are both much higher than in SEM. Accordingly, the main feature that Chorkendorff et al. described in their study was a shrinkage (and not a growth) of most nanoparticles, with only a few of these displaying actual coalescence [22]. Shrinkage in this study was shown to be an effect of both the high electron dose and the oxidizing atmosphere. None of these are characteristic of our SEM measurements; thus in our case, it seems more straightforward to presume that the beam has little effect on the nanocubes themselves, and it is rather the under-beam formation of a carbonaceous passive layer what is seen in Fig. 6.

Although the SEM images recorded at an accelerating voltage of 1.5 kV may not allow a clear distinction between the core of the nanoparticles and the contamination layer formed around them (Figs. 6 and 7a), the contamination layer can be visualized by EM scans at higher (20 kV) accelerating voltage (Fig. 7b). That under the formed carbonaceous contamination layer the Ag nanocubes preserve their original shape can be confirmed by the HAADF–STEM and the TEM bright field images shown in Figs. 7c and d, respectively.

It is of worth noting that the contamination layer is most probably formed by the PVP capping agent, remnants of which remain adsorbed on the Ag nanocubes despite the applied UV–ozone treatment, and then get polymerized and pinned to the electrode surface by the electron beam [28]. Based on the electrocatalytic degradation pattern shown by Fig. 5, we can assume that some PVP may also remain on the substrate, forming there a carbonaceous shell that is however presumed to be not as thick as on the surfaces of the nanocubes, where PVP is primarily adsorbed.

The under-beam formation of the passive layer on the surface of nanoparticulate catalysts seems to block the pre-scanned surface even if entirely different settings, and much harsher electrolysis conditions, compared to what was described before, are applied. This is demonstrated by Fig. 8, where we modified a gas diffusion electrode (GDE) with carbon-supported Ag NCs (this time, without the application of UV-ozone treatment), and performed electrolysis by applying a potential of −1.4 V *vs.* RHE, thus passing through a total charge amount of 1600 C cm^{-2}. While the identical location SEM images of Fig. 8a and b show no trace of degradation, particle deformation and the appearance of newly formed, small particles is clearly shown by the SEM micrograph of Fig. 8c, recorded at a random spot after the electrolysis. Although as pointed out in [40], in fact any organic contaminations of a catalyst sample may act as source of material for the formation of passive carbonaceous crust layers, the prominent role of PVP in this process is further supported by our numerous IL–SEM studies on PVP-free catalysts, where no such contamination effects were ever seen [11–20].

4. Concluding remarks

No effort has so far been made to demonstrate the effect of capping-agent related under-beam passive layer formation on the catalytic behaviour of nanoparticle type electrocatalysts. This is considered worrying, particularly because of the emerging popularity of IL–SEM-based stability studies where the pre-electrolysis scanning can contaminate (and consequently disable) the catalyst sample in a way that the post-electrolysis scan would deceivingly show no degradation.

Using PVP-functionalised Ag nanocubes as model catalysts of CO_2 reduction, we demonstrated how under-beam contamination (a carbonaceous, passive crust formed over the catalyst particles) might account for artefacts in IL–SEM studies in such a way that the experimenter is provided with false comfort with regard to the stability of the catalyst. This paper was written with the aim to direct attention to this possible pitfall of IL–SEM studies, which

may especially emerge when IL–SEM is applied on electrocatalysts prepared by a synthesis route involving capping agents.

Apart from the issues that PVP remnants can cause in the interpretation of IL–SEM experiments, it should also be emphasized that shape-forming surfactants may exert further unwanted effects also on the essential catalytic properties. *E.g.*, in case of the system studied here we have to note that if no action (in our case, UV-ozone treatment) is taken to remove (at least most of) the adhering PVP remnants, this will negatively affect both the selectivity and the stability of the catalyst. In our case omission of the UV-ozone treatment resulted, for example, in the overall Faradaic efficiency (toward CO production) dropping from ~ 80% to ~ 65%, and a further dropping to below 50% over 2 hours of electrolysis (under conditions similar to those applying for Fig. 2b). The removal of capping agents may be based on plasma/thermal annealing [41] (note that the UV-ozone treatment we applied here proved to be far from ideal), or it may even rely on mere electrochemical methods. Namely, it was recently shown in two independent studies (by our group [42] and by Pankhurst et al. [43]) that capping agent remnants may effectively be removed by the harsh cathodic potentials applied during CO_2 electrolysis. Needless to say, the latter "*operando* activation" method [42] does not work for capping agents baked to the catalyst surface by the electron beam in an IL–SEM scenario.

Declaration of Competing Interest

The authors declare that they have no known competing financial interests or personal relationships that could have appeared to influence the work reported in this paper.

Acknowledgement

Support by the CTI Swiss Competence Center for Energy Research (SCCER Heat and Electricity Storage) is gratefully acknowledged. P. B. acknowledges financial support from the Swiss National Foundation (grant 200020–172507). S. V. acknowledges support from the National Research, Development and Innovation Office of Hungary (NKFIH grant FK135375). N. K. and M. de J. G.-V. acknowledge the financial support by the Swiss Government Excellence Scholarships for Foreign Scholars (ESKAS).

References

[1] D.R. Feldman, W.D. Collins, P.J. Gero, M.S. Torn, E.J. Mlawer, T.R. Shippert, Observational determination of surface radiative forcing by CO2 from 2000 to 2010, Nature 519 (7543) (2015) 339–343, https://doi.org/10.1038/nature14240.
[2] S. Nitopi, E. Bertheussen, S.B. Scott, X. Liu, A.K. Engstfeld, S. Horch, B. Seger, I.E. L. Stephens, K. Chan, C. Hahn, J.K. Nørskov, T.F. Jaramillo, I. Chorkendorff, Progress and perspectives of electrochemical CO2 reduction on copper in aqueous electrolyte, Chem. Rev. 119 (12) (2019) 7610–7672, https://doi.org/10.1021/acs.chemrev.8b00705.
[3] E. Royer, Réduction de l'acide carbonique en acide formique, Compt. Rend. Hebd. Séances Acad. Sci. 70 (1870) 731–732.
[4] H.-R.M. Jhong, S. Ma, P.J.A. Kenis, Electrochemical conversion of CO2 to useful chemicals: Current status, remaining challenges, and future opportunities, Curr. Opin. Chem. Eng. 2 (2) (2013) 191–199, https://doi.org/10.1016/j.coche.2013.03.005.
[5] A.D. Handoko, F. Wei, Jenndy, B.S. Yeo, Z.W. Seh, Understanding heterogeneous electrocatalytic carbon dioxide reduction through operando techniques, Nature Catal. 1 (12) (2018) 922–934, https://doi.org/10.1038/s41929-018-0182-6.
[6] A. Bergmann, B. Roldán Cuenya, Operando insights into nanoparticle transformations during catalysis, ACS Catal. 9 (11) (2019) 10020–10043, https://doi.org/10.1021/acscatal.9b01831.
[7] K.J.J. Mayrhofer, J.C. Meier, S.J. Ashton, G.K.H. Wiberg, F. Kraus, M. Hanzlik, M. Arenz, Fuel cell catalyst degradation on the nanoscale, Electrochem. Commun. 10 (8) (2008) 1144–1147, https://doi.org/10.1016/j.elecom.2008.05.032.
[8] N. Hodnik, M. Zorko, M. Bele, S. Hočevar, M. Gaberšček, Identical location scanning electron microscopy: A case study of electrochemical degradation of PtNi nanoparticles using a new nondestructive method, J. Phys. Chem. C 116 (40) (2012) 21326–21333, https://doi.org/10.1021/jp303831c.
[9] N. Hodnik, S. Cherevko, Spot the difference at the nanoscale: Identical location electron microscopy in electrocatalysis, Curr. Opin. Electrochem. 15 (2019) 73–82, https://doi.org/10.1016/j.coelec.2019.03.007.
[10] J.C. Meier, I. Katsounaros, C. Galeano, H.J. Bongard, A.A. Topalov, A. Kostka, A. Karschin, F. Schüth, K.J.J. Mayrhofer, Stability investigations of electrocatalysts on the nanoscale, Energy Environ. Sci. 5 (11) (2012) 9319, https://doi.org/10.1039/c2ee22550f.
[11] M. Rahaman, A. Dutta, A. Zanetti, P. Broekmann, Electrochemical reduction of CO2 into multicarbon alcohols on activated Cu mesh catalysts: An identical location (IL) study, ACS Catal. 7 (11) (2017) 7946–7956, https://doi.org/10.1021/acscatal.7b02234.
[12] A. Dutta, M. Rahaman, M. Mohos, A. Zanetti, P. Broekmann, Electrochemical CO2 conversion using skeleton (sponge) type of Cu catalysts, ACS Catal. 7 (8) (2017) 5431–5437, https://doi.org/10.1021/acscatal.7b01548.
[13] P. Moreno-García, N. Schlegel, A. Zanetti, A. Cedeño López, M.deJ. Gálvez-Vázquez, A. Dutta, M. Rahaman, P. Broekmann, Selective electrochemical reduction of CO2 to CO on Zn-based foams produced by Cu^{2+} and template-assisted electrodeposition, ACS Appl. Mater. Interfaces 10 (37) (2018) 31355–31365, https://doi.org/10.1021/acsami.8b0989.
[14] A. Dutta, C.E. Morstein, M. Rahaman, A. Cedeño López, P. Broekmann, Beyond copper in CO_2 electrolysis: Effective hydrocarbon production on silver-nanofoam catalysts, ACS Catal. 8 (9) (2018) 8357–8368, https://doi.org/10.1021/acscatal.8b01738.
[15] M.deJ. Gálvez-Vázquez, S. Alinejad, H. Hu, Y. Hou, P. Moreno-García, A. Zana, G. K.H. Wiberg, P. Broekmann, M. Arenz, Testing a silver nanowire catalyst for the selective CO2 reduction in a gas diffusion electrode half-cell setup enabling high mass transport conditions, CHIMIA Int. J. Chem. 73 (11) (2019) 922–927, https://doi.org/10.2533/chimia.2019.92.
[16] Y. Hou, S. Bolat, A. Bornet, Y.E. Romanyuk, H. Guo, P. Moreno-García, I.Z. Montiel, Z. Lai, U. Müller, V. Grozovski, P. Broekmann, Photonic curing: Activation and stabilization of metal membrane catalysts (MMCs) for the electrochemical reduction of CO2, ACS Catal. 9 (10) (2019) 9518–9529, https://doi.org/10.1021/acscatal.9b03664.
[17] Y. Hou, R. Erni, R. Widmer, M. Rahaman, H. Guo, R. Fasel, P. Moreno-García, Y. Zhang, P. Broekmann, Synthesis and characterization of degradation-resistant Cu@CuPd nanowire catalysts for the efficient production of formate and CO from CO2, ChemElectroChem 6 (12) (2019) 3189–3198, https://doi.org/10.1002/celc.201900752.
[18] M.deJ. Gálvez-Vázquez, P. Moreno-García, H. Guo, Y. Hou, A. Dutta, S.R. Waldvogel, P. Broekmann, Leaded bronze alloy as a catalyst for the electroreduction of CO2, ChemElectroChem 6 (8) (2019) 2324–2330, https://doi.org/10.1002/celc.201900537.
[19] A.V. Rudnev, K. Kiran, A. Cedeño López, A. Dutta, I. Gjuroski, J. Furrer, P. Broekmann, Enhanced electrocatalytic CO formation from CO_2 on nanostructured silver foam electrodes in ionic liquid/water mixtures, Electrochim. Acta 306 (2019) 245–253, https://doi.org/10.1016/j.electacta.2019.03.102.
[20] A. Dutta, I.Z. Montiel, R. Erni, K. Kiran, M. Rahaman, J. Drnec, P. Broekmann, Activation of bimetallic AgCu foam electrocatalysts for ethanol formation from CO2 by selective Cu oxidation/reduction, Nano Energy 68 (2020) 104331, https://doi.org/10.1016/j.nanoen.2019.104331.
[21] W.T. Osowiecki, J.J. Nussbaum, G.A. Kamat, G. Katsoukis, M. Ledendecker, H. Frei, A.T. Bell, A.P. Alivisatos, Factors and dynamics of Cu nanocrystal reconstruction under CO2 reduction, ACS Appl. Energy Mater. 2 (11) (2019) 7744–7749, https://doi.org/10.1021/acsaem.9b01714.
[22] S.B. Simonsen, I. Chorkendorff, S. Dahl, M. Skoglundh, J. Sehested, S. Helveg, Direct observations of oxygen-induced platinum nanoparticle ripening studied by in situ TEM, J. Am. Chem. Soc. 132 (23) (2010) 7968–7975, https://doi.org/10.1021/ja910094r.
[23] M. Arenz, A. Zana, Fuel cell catalyst degradation: Identical location electron microscopy and related methods, Nano Energy 29 (2016) 299–313, https://doi.org/10.1016/j.nanoen.2016.04.027.
[24] R. Lariviere Stewart, Insulating films formed under electron and ion bombardment, Phys. Rev. 45 (7) (1934) 488–490, https://doi.org/10.1103/physrev.45.488.
[25] M. von Ardenne, Das elektronen-rastermikroskop, Z. Phys. 109 (9–10) (1938) 553–572, https://doi.org/10.1007/bf01341584.
[26] L. Marton, N.N. Das Gupta, C. Marton, Modifications of specimens in electron microscopy, Science 104 (2689) (1946) 35–36, https://doi.org/10.1126/science.104.2689.35.
[27] M.T. Postek, A.E. Vladár, Does your SEM really tell the truth?—How would you know? Part 1, Scanning 35 (6) (2013) 355–361, https://doi.org/10.1002/sca.21075.
[28] M.T. Postek, A.E. Vladár, K.P. Purushotham, Does your SEM really tell the truth?—How would you know? Part 2, Scanning 36 (3) (2013) 347–355, https://doi.org/10.1002/sca.21124.
[29] B. Luo, Y. Fang, J. Li, Z. Huang, B. Hu, J. Zhou, Improved stability of metal nanowires via electron beam irradiation induced surface passivation, ACS Appl. Mater. Interfaces 11 (13) (2019) 12195–12201, https://doi.org/10.1021/acsami.9b00875.
[30] S.F. Tan, M. Bosman, C.A. Nijhuis, Molecular coatings for stabilizing silver and gold nanocubes under electron beam irradiation, Langmuir 33 (5) (2017) 1189–1196, https://doi.org/10.1021/acs.langmuir.6b03721.

[31] S.H. Im, Y.T. Lee, B. Wiley, Y. Xia, Large-scale synthesis of silver nanocubes: The role of HCl in promoting cube perfection and monodispersity, Angew. Chem. 117 (14) (2005) 2192–2195, https://doi.org/10.1002/ange.200462208.
[32] A.V. Rudnev, Online chromatographic detection, in: K. Wandelt (Ed.), Encyclopedia of Interfacial Chemistry, Elsevier, Amsterdam, 2018, pp. 321–325, https://doi.org/10.1016/b978-0-12-409547-2.13564-4.
[33] J. Zhang, Q. Wang, X. Zhang, J. Wang, M. Guo, B.J. Wiley, C. Li, C. Hu, Carbamide promoted polyol synthesis and transmittance properties of silver nanocubes, Inorg. Chem. Front. 3 (4) (2016) 547–555, https://doi.org/10.1039/c5qi00256g.
[34] K.M. Koczkur, S. Mourdikoudis, L. Polavarapu, S.E. Skrabalak, Polyvinylpyrrolidone (PVP) in nanoparticle synthesis, Dalton Trans. 44 (41) (2015) 17883–17905, https://doi.org/10.1039/c5dt02964c.
[35] N. Naresh, F.G.S. Wasim, B.P. Ladewig, M. Neergat, Removal of surfactant and capping agent from Pd nanocubes (Pd-NCs) using tert-butylamine: Its effect on electrochemical characteristics, J. Mater. Chem. A 1 (30) (2013) 8553, https://doi.org/10.1039/c3ta11183k.
[36] D. Ung, B.M. Cossairt, Effect of surface ligands on CoP for the hydrogen evolution reaction, ACS Appl. Energy Mater. 2 (3) (2019) 1642–1645, https://doi.org/10.1021/acsaem.9b00240.
[37] Y. Hori, Electrochemical CO_2 reduction on metal electrodes, in: C.G. Vayenas, R.E. White, M.E. Gamboa-Aldeco (Eds.), Modern Aspects of Electrochemistry, Vol. 42, Springer, New York, 2008, pp. 89–189, https://doi.org/10.1007/978-0-387-49489-0.
[38] D. Sun, X. Xu, Y. Qin, S.P. Jiang, Z. Shao, Rational design of Ag-based catalysts for the electrochemical CO2 reduction to CO: A review, ChemSusChem 13 (2019) 39–58, https://doi.org/10.1002/cssc.201902061.
[39] A. Moysiadou, X. Hu, Stability profiles of transition metal oxides in the oxygen evolution reaction in alkaline medium, J. Mater. Chem. A 7 (45) (2019) 25865–25877, https://doi.org/10.1039/c9ta10308b.
[40] M. Zorko, B. Jozinović, M. Bele, N. Hodnik, M. Gaberšček, SEM method for direct visual tracking of nanoscale morphological changes of platinum based electrocatalysts on fixed locations upon electrochemical or thermal treatments, Ultramicroscopy 140 (2014) 44–50, https://doi.org/10.1016/j.ultramic.2014.02.006.
[41] I. Puspitasari, E. Skupien, F. Kapteijn, P. Kooyman, Au capping agent removal using plasma at mild temperature, Catalysts 6 (2016) 179, https://doi.org/10.3390/catal6110179.
[42] H. Hu, M. Liu, Y. Kong, N. Mysuru, C. Sun, M. d. J. Gálvez-Vázquez, U. Müller, R. Erni, V. Grozovski, Y. Hou, P. Broekmann, Activation matters: Hysteresis effects during electrochemical looping of colloidal Ag nanowire catalysts, ACS Catal. 10 (2020) 8503–8514. https://doi.org/10.1021/acscatal.0c02026.
[43] J.R. Pankhurst, P. Iyengar, A. Loiudice, M. Mensi, R. Buonsanti, Metal–ligand bond strength determines the fate of organic ligands on the catalyst surface during the electrochemical CO2 reduction reaction, Chem. Sci. 11 (2020) 9296–9302, https://doi.org/10.1039/d0sc03061a.